Journal of Energy Storage 181 (2026) 124493

Contents lists available at ScienceDirect

Journal of Energy Storage

journal homepage: www.elsevier.com/locate/est

Research papers

Multifunctional zeolite nanosheet-reinforced polymer electrolytes for high-performance lithium metal batteries

Qian Zhao [a,1], Jiaxin Tu [a,1], Rubing Xu [a,1], Lehao Liu [a,*], Tianrong Yang [a], Rongmin Zhou [a], Dongmei Zhang [a], Mengxuan Zhang [a], Baoyi Wang [a], Dingrong Long [a], Kunda Yang [a], Wei Lv [b], Jianan Gu [a], Lihua Chu [a], Qianxiao Fan [a], Ziyue Wen [a], Bing Jiang [a], Shigang Ling [c], Meicheng Li [a,*]

[a] State Key Laboratory of Alternate Electrical Power System with Renewable Energy Sources, School of New Energy, North China Electric Power University, Beijing, 102206, China
[b] Beijing Laboratory of New Energy Storage Technology, Institute of Energy Power Innovation, North China Electric Power University, Beijing, 102206, China
[c] Beijing Easpring Material Technology Co. Ltd., Beijing, 100160, China

ARTICLE INFO

Keywords:
Poly(ethylene oxide) electrolyte
MFI zeolite nanosheet
Lithium metal battery
Ionic conductivity

ABSTRACT

The incorporation of inorganic nanofillers is considered as a facile approach for enhancing the functionality of solid polymer electrolytes; however, the ionic conductivity and electrochemical stability remain insufficient for practical applications in lithium metal batteries, owing to the nanofillers' small specific surface area and inadequate interactions with polymer matrices/lithium salts. In this study, two-dimensional MFI zeolite nanosheets with abundant micro- and meso-pores, hydroxyl groups, and Lewis acidic sites are prepared as a multifunctional nanofiller to alter electrolytes based on poly(ethylene oxide) (PEO). The hydroxyl-modified zeolite nanosheets have hydrogen bonding with the ether oxygen groups of PEO, thereby reducing the PEO crystallinity and facilitating fast segment movement. Meanwhile, the abundant Lewis acidic sites on the nanosheets with a large specific surface can anchor anions of lithium bis(trifluoromethanesulfonyl)imide (LiTFSI), which would facilitate the LiTFSI dissociation for releasing more free Li^+. Consequently, the room-temperature ion conductivity and Li^+ transference number of the polymer electrolyte increase to 6.35×10^{-5} S cm^{-1} and 0.55, indicating enhancements of around 3 and 4 times in comparison to the unaltered electrolyte, respectively. In addition, the electrochemical stability window of the electrolyte increases from 4.2 V to 5.0 V, and the thermostability and Young's modulus are also strengthened. Therefore, the cycling lifespan of the Li||Li battery increases from 352 h to 2719 h at 0.1 mA cm^{-2}. Additionally, the Li||$LiFePO_4$ battery utilizing the nanosheet-enhanced electrolyte demonstrates a greater capacity retention ratio of 93.1% after long-time cycling. The work offers a novel approach for reinforcing polymer electrolytes through the incorporation of multifunctional zeolite nanosheets for high-performance lithium metal battery applications.

1. Introduction

Owing to their distinct merits, including a long cycling life and low cost, Li-ion batteries (LIBs) are widely utilized in drones, electric vehicles, and handheld electronics [1]. However, the energy density of LIBs remains insufficient to satisfy the energy storage requirements of the current market [2]. In addition, liquid non-aqueous electrolytes such as carbonates and organic ethers have a few obvious disadvantages, such as easy leakage and flammability, which pose challenges to the safety of LIBs [3]. The implementation of solid-state electrolytes in LIBs, as opposed to conventional liquid electrolytes, is seen to be a successful strategy for improving safety. Concurrently, this strategy facilitates an increase in energy density by enabling the utilization of high-voltage cathodes and high-capacity lithium metal anodes [4,5].

Solid-state electrolytes are often classified into two categories: inorganic ceramic electrolytes and organic polymer electrolytes. Inorganic ceramic electrolytes offer remarkable electrochemical stability and an ionic conductivity of 10^{-2}–10^{-4} S cm^{-1} at room temperature [6].

* Corresponding authors.
E-mail addresses: lehaoliu@ncepu.edu.cn (L. Liu), mcli@ncepu.edu.cn (M. Li).
[1] Qian Zhao, Jiaxin Tu and Rubing Xu contribute equally to this paper.

https://doi.org/10.1016/j.est.2026.124493
Received 26 January 2026; Received in revised form 15 August 2026; Accepted 28 August 2026
2352-152X/© 2026 Elsevier Ltd. All rights are reserved, including those for text and data mining, AI training, and similar technologies.

However, the high impedance at the electrode/electrolyte interface restricts their application in LIBs. On the contrary, solid polymer electrolytes are readily fabricated and exhibit high flexibility, which facilitates enhanced interaction at the electrolyte/electrode interface [7,8]. Nevertheless, polymer electrolytes have a few problems, such as low ambient-temperature ion conductivity (10^{-6}–10^{-8} S cm^{-1}) and weak electrochemical oxidation stability, which cause poor cycling performance of LIBs [9–12].

To satisfy the stringent demands of solid-state lithium metal batteries (LMBs), many important strategies including molecular crosslinking [13–16], polymer blending [17–19], copolymerization [20–22], adding plasticizers [5,23,24], and adding inorganic nanofillers [25–29] are utilized to enhance the ionic conductivity and oxidation stability of polymer electrolytes. For example, inorganic nanoparticles usually engage in Lewis acid-base interactions with polymeric matrices and lithium salts, which can boost lithium salt dissociation to release free Li^+, and meanwhile increase the amorphous areas of polymer matrices, thus enhancing the conductivity of ions [28,30]. Nevertheless, the ambient-temperature ion conductivity and the electrochemical stability of composite polymer electrolytes are still insufficient for practical application in LMBs [31]. This limitation is primarily attributed to the restricted specific surface area of inorganic nanofillers and their weak interactions with both the polymeric matrices and lithium salts. Thus, it is required to develop multifunctional nanoparticles with a large specific area and abundant functional groups as nanofillers to greatly enhance the electrical and electrochemical performance of polymer electrolytes [32,33].

In this study, two-dimensional MFI zeolite nanosheets with micro- and meso-pores and numerous hydroxyl groups are exploited as a multifunctional nanofiller for improving the overall properties of poly (ethylene oxide) (PEO)-lithium bis(trifluoromethanesulfonyl)imide (LiTFSI) electrolytes (Fig. 1a). The hydrogen-bonding interactions between the hydroxyl groups on the large-surface-area zeolite nanosheets and the ether oxygen atoms of PEO would suppress the crystallization of PEO, thereby enhancing the mobility of polymer chains (Fig. 1b). Based on Lewis acid-base theory, the Lewis acid sites (e.g., aluminum atoms) on the nanosheets are beneficial for anchoring $TFSI^-$ to emancipate more free Li^+ from LiTFSI. Thus, the ionic conductivity and the Li^+ transference number of the polymer electrolytes greatly increase. Meanwhile, the electrochemical stability window and mechanical robustness of the electrolytes are reinforced, because of the interactions between the porous zeolite nanosheets and PEO/$TFSI^-$. As a result, the zeolite nanosheet-containing composite polymer electrolytes (denoted as PEO-LiTFSI-Zeo) exhibit much higher resistance to lithium dendrite growth. Additionally, the solid-state LMBs based on the composite electrolyte demonstrate exceptional cycle stability and rate performance.

2. Experimental section

2.1. Preparation of zeolite

The surfactant of $(C_{22}H_{45}\text{-}N^+(CH_3)_2\text{-}C_6H_{12}\text{-}N^+(CH_3)_2\text{-}C_6H_{13})Br_2$ (denoted as $C_{22\text{-}6\text{-}6}Br_2$) was synthesized with reference to the literature [34,35], and its structure was confirmed by ^{1}H NMR characterization. Zeolite nanosheets were prepared via a hydrothermal method according to the chemical composition of $30Na_2O/1Al_2O_3/100SiO_2/10C_{22-6-6}Br_2/4000H_2O/18H_2SO_4$ [36]. The preparation process was as follows. NaOH, H_2SO_4, $Al_2(SO_4)_3{\cdot}16H_2O$, and tetraethyl orthosilicate (TEOS) were sequentially mixed and stirred. The resulting mixture was then combined with the $C_{22-6-6}Br_2$ solution, transferred into an autoclave, and crystallized at 423 K for 60 h. After crystallization, the product was filtered, washed, and dried, followed by calcination in dry air at 873 K. Subsequently, the calcined product was subjected to ion exchange using a 1 M NH_4Cl aqueous solution, then centrifuged, washed, and dried [37]. Detailed operating parameters are provided in

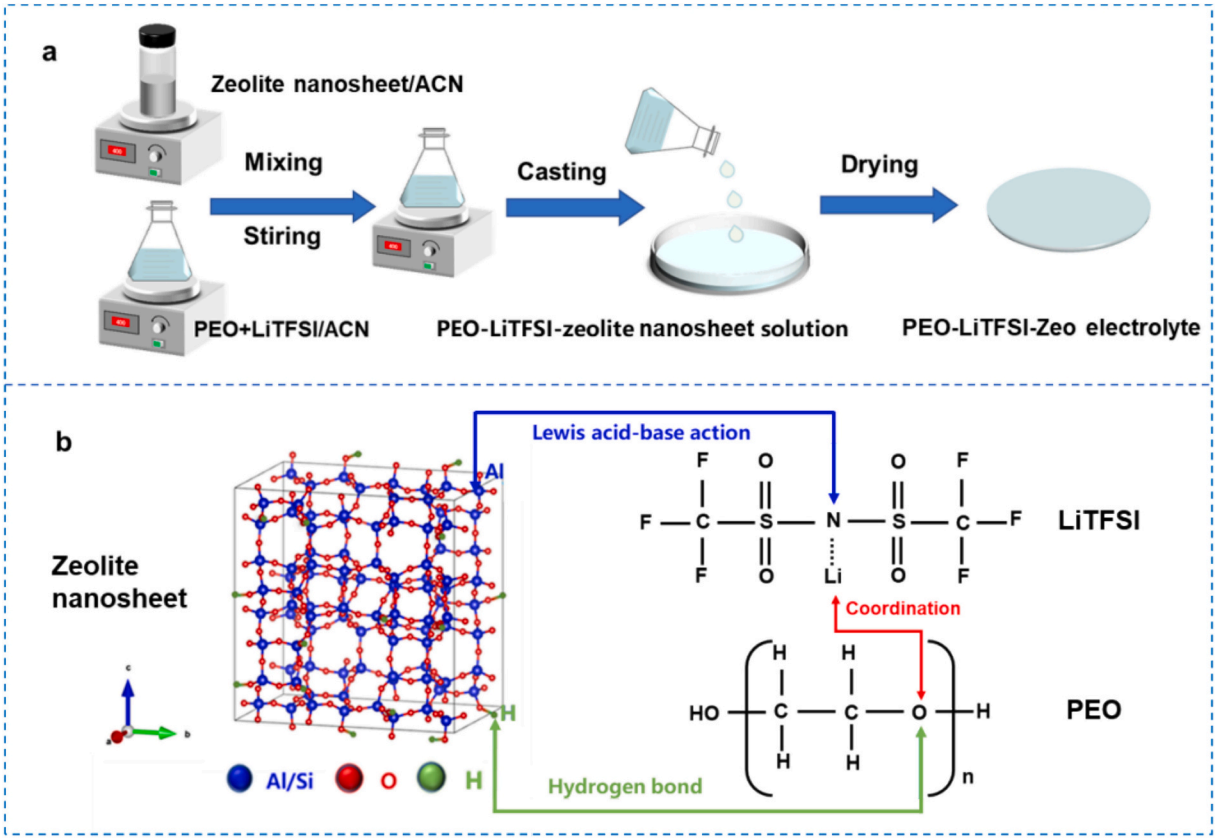


Fig. 1. (a) Schematic explanation of the solution casting procedure for preparing PEO-LiTFSI-Zeo electrolytes, and (b) PEO/LiTFSI-zeolite interactions.

Text S1 (Supporting Information).

2.2. Preparation of PEO-LiTFSI-zeolite electrolytes

Different masses of zeolite nanosheets (0, 0.025, 0.077, 0.132, and 0.188 g) were respectively dispersed in acetonitrile, followed by ultrasonic treatment and stirring. Separately, PEO (molecular weight: 600,000) and LiTFSI were dissolved in acetonitrile at a molar ratio of EO: Li^+ = 18:1 and stirred. The two solutions were then mixed and stirred, after which the mixture was cast into Teflon molds and dried under vacuum at 60 °C for 72 h to prepare composite electrolyte membranes of PEO-LiTFSI-Zeo. These membranes were named Zeo0, Zeo1, Zeo3, Zeo5, and Zeo7, according to the mass fractions of zeolite nanosheets of 0, 1, 3, 5, and 7 wt%, respectively. When the electrolyte membranes were cut into discs, they were stored in a glove box with both water and oxygen contents of <0.1 ppm. The thickness of the composite electrolyte membranes was 190–230 μm. Detailed operating parameters are provided in Text S2.

2.3. Material characterizations

Full descriptions of material characterizations, including equipment specifications and operational parameters, are provided in Text S3.

2.4. Electrochemical measurements

Complete details of electrochemical measurements are documented in Text S4.

3. Results and discussion

3.1. Microstructure and morphology of nanosheets and electrolytes

To characterize the phase composition of the zeolite nanosheets,

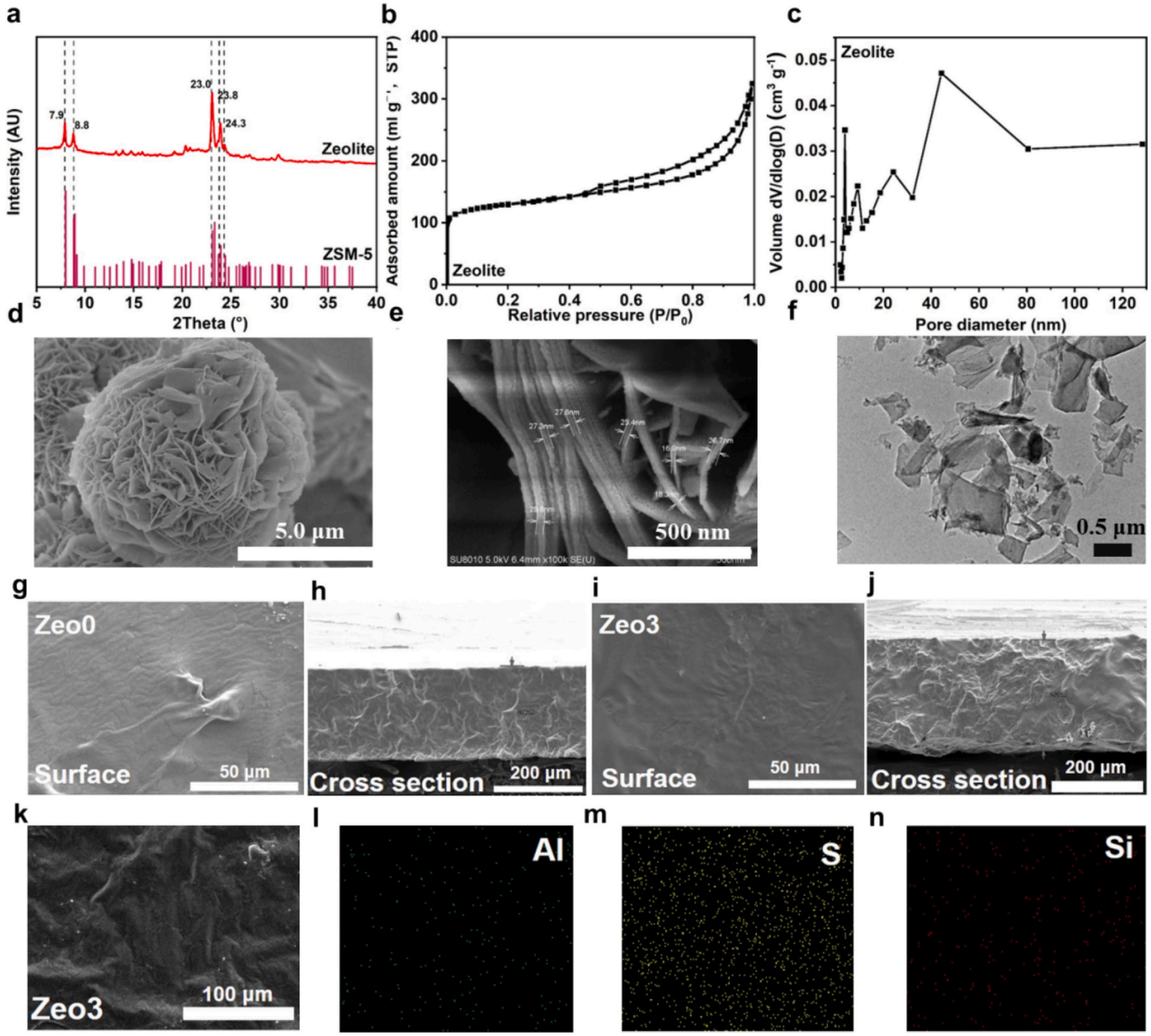


Fig. 2. Microstructure of zeolite nanosheets and polymer electrolytes. (a) XRD patterns, (b) adsorption-desorption isotherms of N_2, (c) pore size distribution, (d–e) SEM images, and (f) TEM image of zeolite nanosheets. SEM images of (g–h) Zeo0 and (i–j) Zeo3 electrolytes at the surface (g and i) and the cross section (h and j). EDS mapping images of (l) Al, (m) S, and (n) Si elements in Fig. 2k.

their X-ray diffraction (XRD) patterns are presented in (Fig. 2a). The freshly formed zeolite nanosheets show a few typical diffraction peaks at 7.9, 8.8, 23.0, 23.8, and 24.3° [38]. The zeolite nanosheets also have an enormous specific surface area of 488.57 m^2 g^{-1} (Fig. 2b) and an average mesoporous diameter of 9.19 nm (Fig. 2c), indicating the successful preparation of the porous MFI zeolite.

Scanning electron microscope (SEM) was then employed for direct visualization of the zeolite nanosheets (Fig. 2d–e). The zeolite nanosheet assemblies are spherical, exhibiting an average size of 9 μm and thicknesses of 20–40 nm. Transmission electron microscopy (TEM) testing further shows that the nanosheet assemblies are easily crushed into nanosheets after sonication for several minutes, and they show a sheet-like structure with thin thicknesses (Fig. 2f). The surface and cross-sectional morphology of the polymer electrolytes was revealed by SEM (Figs. 2g–k and S1), and the zeolite nanosheet-containing composite electrolyte have similar surfaces and cross sections to the Zeo0 electrolyte. The EDS mappings of Al and Si elements further prove the uniform dispersion of the zeolite nanosheets in the PEO-LiTFSI matrices (Fig. 2k–n), which would be advantageous for improving the electrolyte properties.

3.2. Ion conductance of electrolytes

To establish the quantitative relationship between zeolite nanosheet content and the ionic conductivity of the PEO-based electrolytes, the electrochemical impedance spectroscopy (EIS) spectra were obtained at various temperatures ranging from 30 to 80 °C (Fig. S2). The Zeo0 electrolyte has an ionic conductivity of 2.22 × 10^{-5} S cm^{-1} at 30 °C (Fig. 3a). As the content of the zeolite nanosheets increases, the room-temperature ionic conductivities increase to 5.27 × 10^{-5}, 6.35 × 10^{-5}, 4.62 × 10^{-5}, and 4.06 × 10^{-5} S cm^{-1} for the Zeo1, Zeo3, Zeo5, and Zeo7 electrolytes, respectively. The decrease in the ionic conductivity of the electrolytes with the high contents of 5–7 wt% may be ascribed to the aggregation of the zeolite nanosheets and the disruption of the ionic transport pathways. To further elucidate the ion transport mechanism, we fitted the ionic conductivities at various temperatures by using the Arrhenius equation. With the addition of zeolite, the activation energies (E_a) decreased from 0.81 eV (Zeo0) to 0.70 (Zeo1) and 0.68 eV (Zeo3). This reduction in E_a value indicates that the incorporation of the zeolite particles lowers the energy barrier for ion migration, thereby facilitating the ion transport and enhancing the ionic conductivity [39,40].

XRD and differential scanning calorimetry (DSC) were applied to investigate how the zeolite nanosheets influence the ionic conductivity of the composite electrolytes. In the original Zeo0 electrolyte, several characteristic XRD peaks appeared at 19.1° and 23.4°, corresponding to the crystallization of PEO. However, the intensity of these peaks was significantly reduced in the Zeo1 and Zeo3 composite electrolytes (Fig. 3b), indicating that the zeolite nanosheets effectively inhibited the PEO crystallization. The DSC measurements (Fig. 3c) further demonstrate that the PEO crystallinity of the Zeo3 electrolyte is 27.5%, which is lower than that of the Zeo0 electrolyte (34.0%). These findings demonstrate that the zeolite nanosheets are crucial for restricting the PEO crystallization, which promotes the movement of the PEO chains and the increase of the ionic conductivity.

To further clarify how the zeolite nanosheets function, Fourier transform infrared (FT-IR) absorbance spectroscopy was performed as a complementary characterization technique (Fig. 3d). PEO shows a few peaks at 1100 cm^{-1}, and 1340 and 2880 cm^{-1} assigned to the vibration of C-O-C, and asymmetric and symmetric stretching vibrations of -CH_2-, respectively; however, these peak intensity in the Zeo0 electrolyte decreases with the addition of LiTFSI, because of the connection between Li^+ and the ether oxygen groups of PEO [1]. For both Zeo0 and Zeo3 electrolytes, the peaks corresponding to stretching vibrational modes of S═O (1341 cm^{-1}) and N-S (1050 cm^{-1}) change to 1342 cm^{-1} and 1053 cm^{-1}, respectively, which can be attributed to the interaction between the Lewis acidic sites in the zeolite nanosheets and $TFSI^-$ anions [41]. Additionally, for both Zeo0 and Zeo3 electrolytes, the characteristic C-

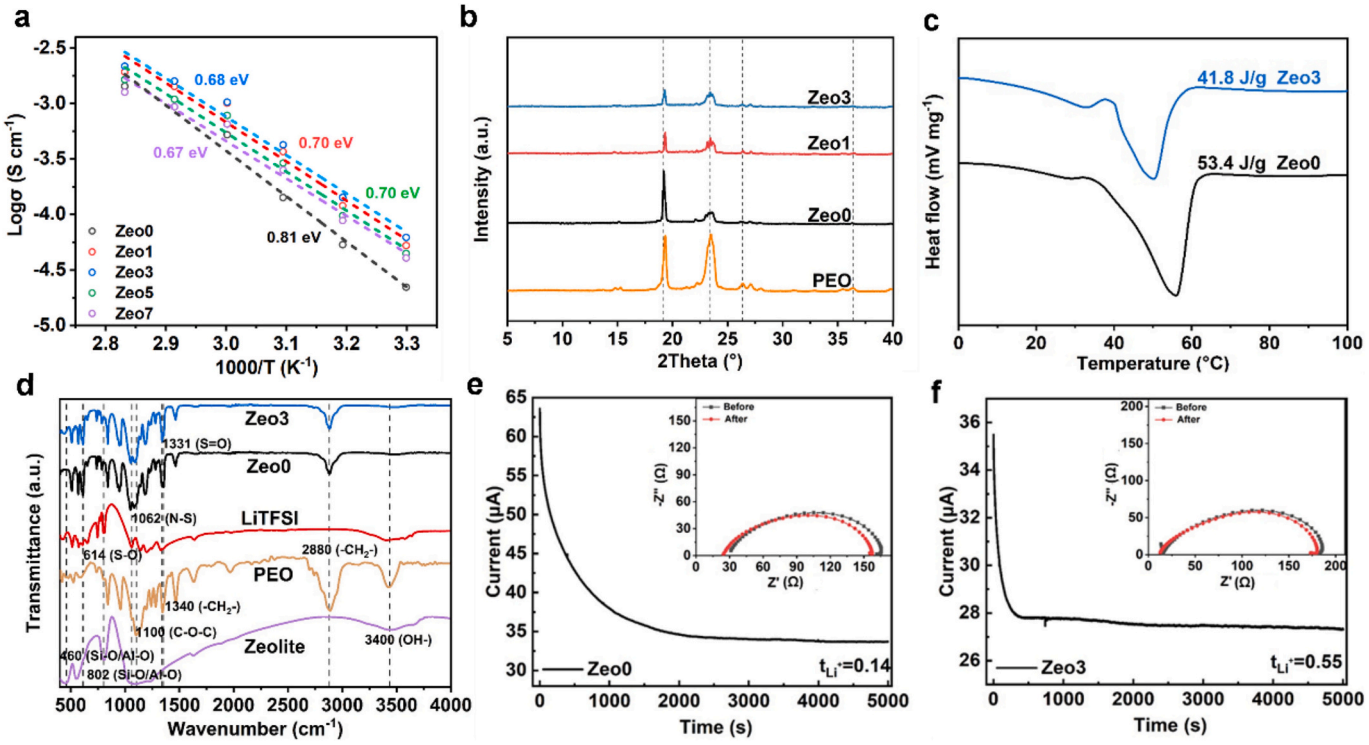


Fig. 3. Electrical properties of electrolytes. (a) Arrhenius plots and activation energies of electrolytes. (b) XRD patterns of PEO and electrolytes. (c) DSC curves of Zeo0 and Zeo3 electrolytes. (d) FT-IR spectra of zeolite nanoparticles, PEO, LiTFSI, Zeo0 and Zeo3 electrolytes. Chronoamperometry profiles of Li||Li symmetric cells with (e) Zeo0 and (f) Zeo3 electrolytes at 60 °C (Inset: Pre- and post-polarization EIS data).

O-C stretching peak of PEO shifts from 1087 cm^{-1} to 1095 cm^{-1}, accompanied by the change of the −OH peak of zeolite at 3400 cm^{-1} [42]. These spectral changes clearly demonstrate the presence of hydrogen bonding interactions between the −OH groups of zeolite and the ether oxygen groups of PEO chains. Thus, the Zeo1 and Zeo3 electrolytes show much higher Li^+ transference numbers of 0.42 and 0.55 than the pristine Zeo0 electrolyte (0.14), respectively (Figs. 3e–f and S3), which would be beneficial for reducing the concentration polarization during the battery cycling process and driving the uniform deposition of Li^+ on the lithium electrodes.

In short, in the pure Zeo0 electrolyte, Li^+ moves along with the ether oxygen atoms in amorphous PEO domains, largely relying on the segmental motion of PEO chains. However, in the composite electrolytes, the hydrogen bonding interaction between the −OH groups of the zeolite nanosheets and the ether oxygen groups of PEO reduces the PEO crystallinity, and meanwhile the Lewis acid-base interaction between the Lewis acidic sites (Al^{3+}) in the zeolite nanosheets and $TFSI^-$ facilitates the LiTFSI dissociation, resulting in the increase in both PEO segmental movement capability and Li^+ concentration at the nanofiller/PEO interfaces, and then the formation of fast ion transport channels at the nanofiller/PEO interfaces. Thus, the Zeo3 composite electrolyte exhibits higher ionic conductivity and Li^+ transference number than the pristine Zeo0 electrolyte.

3.3. Mechanical and electrochemical properties of electrolytes

Linear sweep voltammetry (LSV) tests were conducted at 60 °C to investigate how zeolite nanosheets affect the electrochemical window of composite electrolytes (Fig. 4a). The Zeo0 electrolyte shows an oxidation stabilization potential of ~4.2 V. In comparison, the composite electrolytes exhibit much higher oxidation stabilization potentials of ~5.0 V, implying a significantly improved electrochemical stability of the composite electrolyte after zeolite addition [4]. This should be ascribed to the Lewis acid-base coordination between $TFSI^-$ (Lewis base) and the Lewis acidic sites of the zeolite, which effectively hinders the $TFSI^-$ decomposition [43]. In addition, the hydrogen bonding between the hydroxyl groups on the zeolite nanosheets and the ether oxygen groups in PEO would be helpful for inhibiting the decomposition of PEO.

The tensile test of the electrolyte films was performed as well (Fig. 4b). The ultimate tensile strength and Young's modulus of the Zeo0 electrolyte are 1.08 and 0.66 MPa, respectively. With the incorporation of zeolite, the ultimate tensile strength of the electrolyte membranes decreases, but the Young's modulus increases to 1.63 MPa (the Zeo3 electrolyte, Fig. 4c), due to the high rigidity of the inorganic zeolite. Composite electrolytes with improved Young's modulus offer an advantage in inhibiting lithium dendrite formation in LMBs.

Fig. 4d presents the thermogravimetric analysis (TGA) curves of the Zeo0 and Zeo3 electrolytes. Considering the boiling points of acetonitrile (82 °C) and water (100 °C), the slight weight loss of less than 1.5 wt % observed below 100 °C indicates that only a small amount of volatile species (i.e., residual acetonitrile and moisture) remained in the polymer electrolyte membranes. The primary weight loss at ~390 °C was attributed to the decomposition of PEO, whereas the weight loss occurring between 100 and 250 °C arose from the thermal decomposition of the lithium salt. At 700 °C, the Zeo0 and Zeo3 electrolytes maintained residual amounts of 3.6 and 8.0 wt%, respectively. The difference in the residual amounts (4.4%) was consistent with the weight content of the zeolite nanosheets (3%) in the Zeo3 composite electrolyte. The increase in the residual amount of the Zeo3 electrolyte

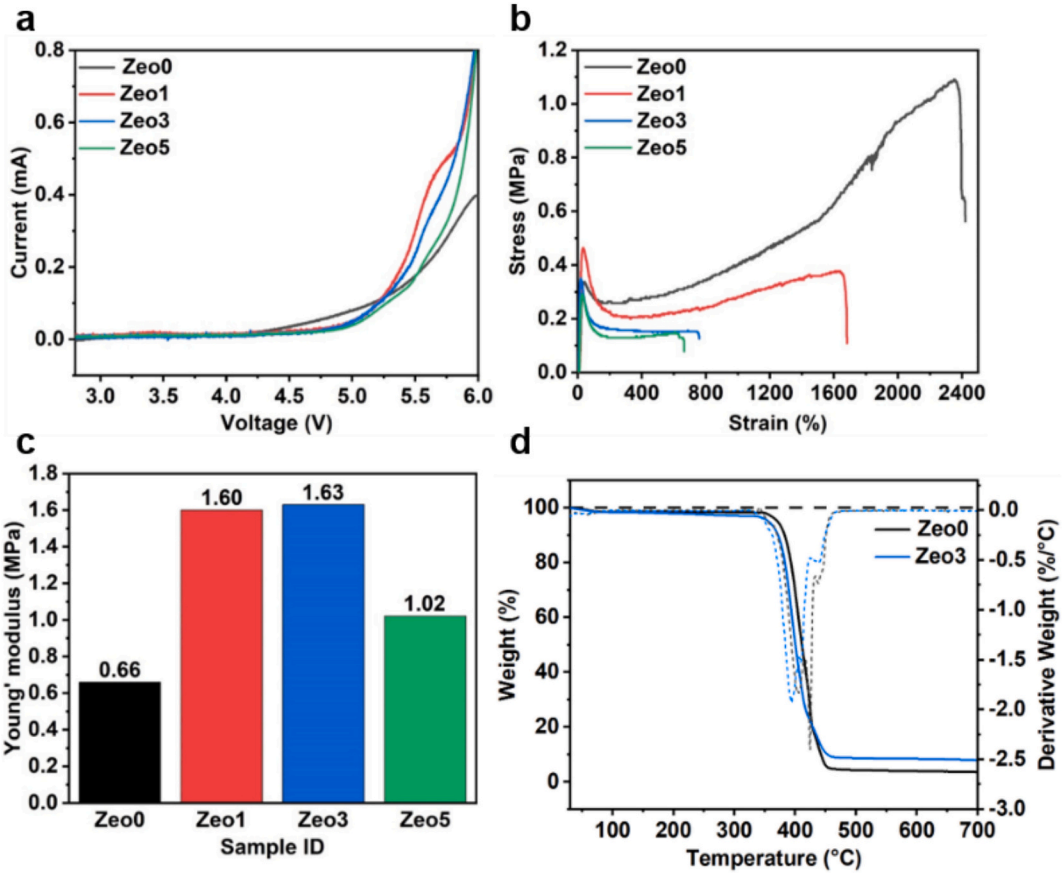


Fig. 4. (a) LSV curves, (b) stress-strain curves, and (c) Young's modulus of electrolytes. (d) TGA and DTG curves of the Zeo0 and Zeo3 electrolytes (solid and dashed lines represent TGA and DTG curves, respectively).

(1.4%) at 700 °C may be attributed to the hydrogen-bonding and Lewis acid-base interactions between zeolite nanosheets and PEO-LiTFSI matrices (Fig. 3d), which can alter the PEO-LiTFSI thermal decomposition behaviors.

3.4. Lithium dendrite resistance of electrolytes

To evaluate the inhibitory effect of the composite electrolytes on lithium dendrite formation, charge and discharge testing were performed on the Li||Li symmetric cells at 60 °C with stepwise increasing current densities (Figs. 5a–c and S4a). The Zeo0 electrolyte-based battery has a critical current density (CCD) of 0.5 mA cm^{-2}, while the Li||Li batteries based on the Zeo1, Zeo3 and Zeo5 electrolytes have higher CCDs of 0.6, 0.8 and 0.6 mA cm^{-2}, respectively. Moreover, the Li||Li cells utilizing the Zeo1 and Zeo3 electrolytes exhibit potentials of 240 and 130 mV, respectively, both of which are much lower than the potential of the battery employing the Zeo0 electrolyte (270 mV), when operated at 0.4 mA cm^{-2}. These findings indicate that the filling of the zeolite nanosheets can significantly increase the electrolyte/electrode contact stability.

Durability tests were conducted on Li||Li batteries based on the electrolytes at 0.1 mA cm^{-2} (with an areal capacity of 0.10 mAh cm^{-2}) (Figs. 5d–f and S4b). The potential of Li||Li battery based on Zeo0 electrolyte dropped sharply after 352 h, demonstrating that the battery easily short-circuited (Fig. 5d). Conversely, the Li||Li batteries utilizing the Zeo1 and Zeo3 electrolytes demonstrated much longer cycling life of 2227 and 2719 h, respectively (Fig. 5e–f). This greatly enhanced stability is likely attributable to the improved electrical and mechanical properties of the composite electrolytes conferred by the incorporation of the zeolite nanosheets (Fig. 3a and c).

The EIS spectra of the Li||Li symmetric batteries prior to and following the cycling are shown in Fig. S4c–e. In the high-frequency regions, the observed semicircle corresponds to the electrolyte-lithium electrode interfacial resistance (R_i). Notably, the R_i value of the battery utilizing the Zeo0 electrolyte increased from 280 Ω to 594 Ω after 352 h of cycling (Fig. S4c), which may be ascribed to accumulation of electrolyte decomposition byproducts and uneven lithium deposition, leading to interface contact loss. On the contrary, the R_i value of the Zeo3 electrolyte-based battery only increased from 196 to 322 Ω after the cycling for 2719 h (Fig. S4e). This further indicates that the inclusion of the zeolite nanosheets can significantly improve the interfacial stability.

SEM observations were conducted to investigate the surface morphology of lithium metal electrodes after cycling. There are many lithium dendrites on the surface of the cycled lithium electrodes paired with the Zeo0 electrolyte (Fig. 5g), which also explains the short-circuiting phenomenon during the galvanostatic cycling process (Fig. 5d) and the high interface resistance (Fig. S4c). In comparison, there are few lithium dendrites on the lithium electrodes paired with the Zeo1, Zeo3 and Zeo5 electrolytes (Figs. 5h–i and S4f), again indicating that the zeolite nanosheets can effectively suppress the lithium dendrite growth.

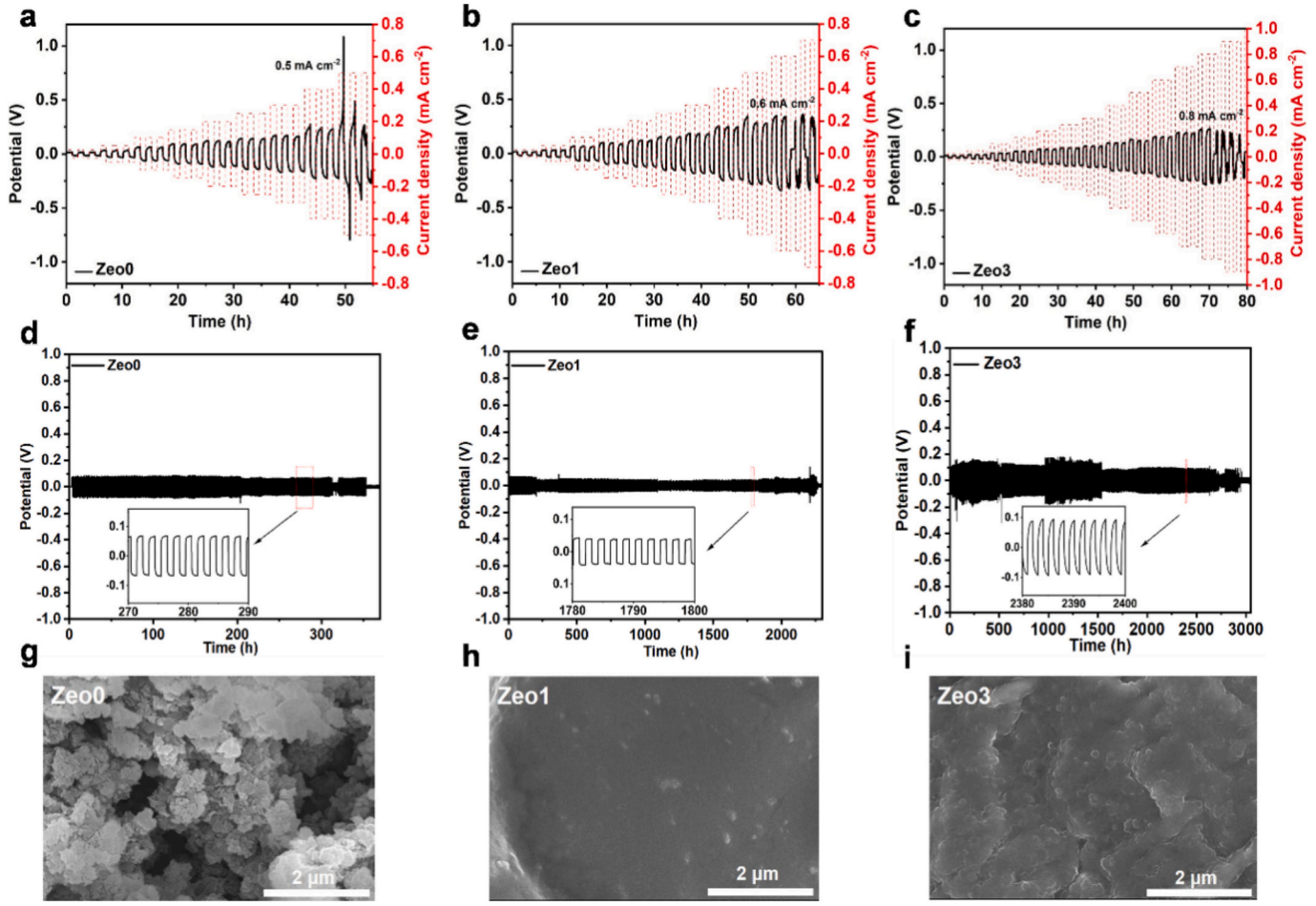


Fig. 5. Resistance ability against lithium dendrites. Critical current density test of Li||Li cells with (a) Zeo0, (b) Zeo1 and (c) Zeo3 electrolytes at 60 °C. Galvanostatic cycling curves of Li||Li cells with (d) Zeo0, (e) Zeo1 and (f) Zeo3 electrolytes at 60 °C (Inset: Enlarged charge-discharge curves). SEM images of post-galvanostatic-cycled Li electrodes from Li||Li cells with (g) Zeo0, (h) Zeo1 and (i) Zeo3 electrolytes.

3.5. LMB cycling performance

Solid-state LMBs with the Li||$LiFePO_4$ configuration were fabricated and subjected to electrochemical testing at 60 °C and various current rates to assess the practical applicability of the electrolytes in LMBs (Fig. 6a). The Zeo1 (151, 151, 150, 147 and 133 mAh g^{-1}) and Zeo3 (154, 153, 150, 143 and 84 mAh g^{-1}) electrolyte-based batteries showed much higher discharge capacities than the Zeo0 electrolyte-based

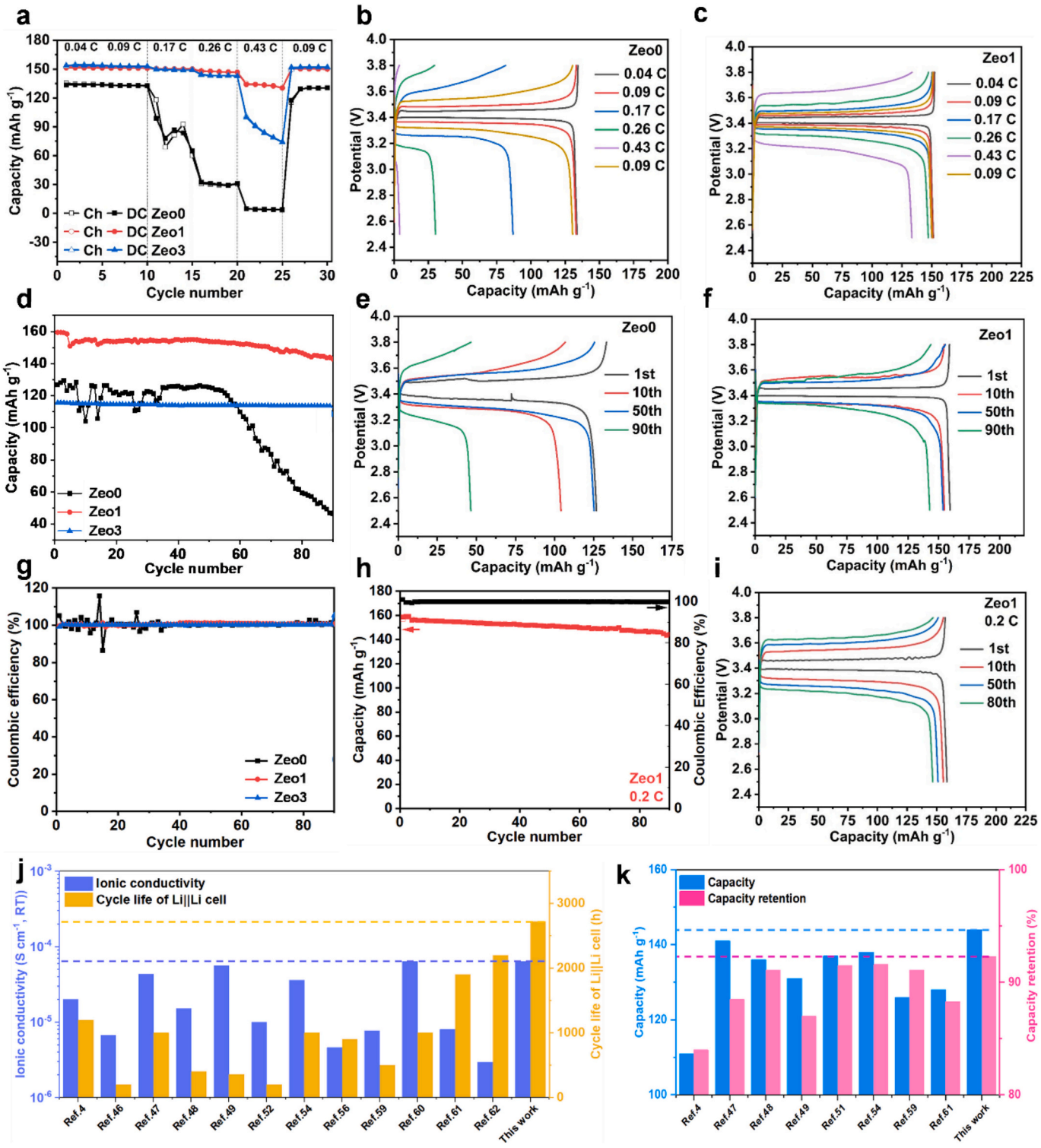


Fig. 6. Solid-state LMB cycling performance. (a) Rate performance of Li||$LiFePO_4$ cells at 60 °C, and the voltage profiles during charge and discharge processes of (b) Zeo0 and (c) Zeo1 electrolyte-based batteries at different rates. (d) Cycling performance of Li||$LiFePO_4$ cells at 0.09C, and the voltage profiles during charge and discharge processes of (e) Zeo0 and (f) Zeo1 electrolyte-based batteries at 0.09C. (g) Coulombic efficiencies of Li||$LiFePO_4$ batteries at 0.09C. (h) Cycling performance of Li||$LiFePO_4$ cells at 0.2C, and (i) the voltage profiles during charge and discharge processes of Zeo1 electrolyte-based battery. Comparison of (j) electrical properties of electrolytes and Li||Li battery performance, and (k) Li||$LiFePO_4$ battery performance recently reported in open literatures. More details are given in Table S1.

battery (133, 133, 78, 30 and 4 mAh g^{-1}) at 0.04, 0.09, 0.17, 0.26 and 0.43C, respectively, because of the high ionic conductivity and Li^+ transference number of the nanosheet-containing electrolytes (Figs. 3a, f and S3a). After 25 cycles, the current density reverted to 0.09C, the batteries with the composite electrolyte-based batteries retained satisfactory capacities. Moreover, the batteries with the composite electrolytes also showed much lower polarization than the battery with the Zeo0 electrolyte, regardless of measured rates (Figs. 6b–c and S5a).

The Li||$LiFePO_4$ batteries were subjected to galvanostatic cycling at a rate of 0.09C and a temperature of 60 °C to evaluate their long-term cycling stability. (Figs. 6d–g and S5b). During 90 cycles, the discharge capacity of the battery utilizing the pristine Zeo0 electrolyte exhibited a rapid decline from 126 to 47 mAh g^{-1}, corresponding to a capacity retention of 37.3%. On the contrary, the battery employing the Zeo1 electrolyte demonstrated superior cycling performance with an original capacity of 160 mAh g^{-1} and a capacity retention of 89.4% (143 mAh g^{-1}) after 90 cycles (Fig. 6d). The battery containing the Zeo3 electrolyte had an original capacity of 116 mAh g^{-1} and retained 108 mAh g^{-1} after 90 cycles, achieving a capacity retention of 93.1%. The initial capacity of the Zeo3 electrolyte-based battery is lower than those of the Zeo0 and Zeo1 electrolyte-based batteries, which is mainly attributed to the increase in the rigidity of the Zeo3 composite electrolyte, and the deterioration of the interfacial contact between the Zeo3 electrolyte and the electrodes. EIS characterizations further showed that the interfacial resistance (R_i) of the Zeo0 electrolyte-based battery increased greatly from 1080 Ω to 5078 Ω after cycling, while the Zeo1 electrolyte-based battery had lower R_i values of 975 and 3181 Ω before and after the cycling, respectively (Fig. S6), indicating the enhanced electrolyte/electrode interfacial stability with the appropriate incorporation of the zeolite nanosheets.

When cycled at 0.2C, the Zeo1 electrolyte-based battery had an original discharge capacity of 156 mAh g^{-1}, and the capacity decreased to 144 mAh g^{-1} after 90 cycles with high capacity retention of 92.3% and Coulombic efficiencies of ~100% (Fig. 6h–i), which should be ascribed to the high ionic conductivity, excellent Young's modulus and enhanced resistance against lithium dendrites of the composite electrolytes. Furthermore, X-ray photoelectron spectroscopy (XPS) was used to analyze the composition of the solid electrolyte interphase (SEI) formed on the lithium metal anodes after electrochemical cycling in Li||$LiFePO_4$ cells with the Zeo0 and Zeo1 electrolytes. As shown in Fig. S7, significant differences in the chemical composition of SEI were observed between the two electrolyte systems. Generally, high-modulus LiF and high-ionic conductivity Li_3N are considered as effective inorganic components to improve interfacial stability and lithium dendrite resistance. Similarly, Li_2CO_3 is also a dense inorganic component with higher modulus and ionic conductivity than organic SEI species, which is beneficial for blocking side reactions between lithium metal electrodes and polymer electrolytes and preventing SEI film fracture. The SEI derived from the Zeo0 electrolyte-paired lithium electrode is rich in organic species (ROLi) and contains a large amount of residual LiTFSI [6]. In contrast, the Zeo1 composite electrolyte promoted the formation of inorganic components including LiF, Li_3N, and Li_2CO_3, which endowed the battery with improved interfacial stability and dendrite resistance [4,5,44,45]. The zeolite nanosheet-filled composite electrolyte delivers comprehensively-improved properties including Li^+ transference number of 0.55, Li||Li cell cycling life of 2719 h, and Li||$LiFePO_4$ battery cycling performance, which are comparable to the best levels reported in recently published literatures (Fig. 6j–k and Table S1) [4,46–62].

To evaluate the electrochemical compatibility of the composite electrolytes with high-voltage $LiNi_{0.6}Co_{0.2}Mn_{0.2}O_2$ cathode and their practical application potential, long-term cycling of Li||$LiNi_{0.6}Co_{0.2}Mn_{0.2}O_2$ cells was first performed at 30 °C and 0.1C (Fig. S8). The Zeo0-based cell delivered an initial capacity of 143.1 mAh g^{-1} and failed completely after 57 cycles with capacity dropping to 0 mAh g^{-1}. By contrast, the Zeo1-based cell exhibited an initial discharge capacity of 206.8 mAh g^{-1}, retaining 116.1 mAh g^{-1} after 86 cycles with Coulombic efficiencies close to 100%, demonstrating superior interfacial stability of the Zeo1 electrolyte at room temperature. Further testing was conducted at a higher temperature of 60 °C and 0.1C. As shown in Fig. S9, the capacity of the Zeo0-based cell decreased to 95 mAh g^{-1} after 19 cycles. In contrast, the capacity of the Zeo1-based cell slowly decreased to 95 mAh g^{-1} after 47 cycles and still retained 76 mAh g^{-1} after 60 cycles. Moreover, the charge-discharge voltage profiles reveal significantly lower polarization of the Zeo1-based cell compared to the Zeo0-based cell (Fig. S10). These results demonstrate that the Zeo1 composite electrolyte with the enhanced interfacial compatibility shows great application potential in the high-voltage LMBs.

4. Conclusions

For the first time, porous zeolite nanosheets were utilized as a versatile nanofiller for enhancing the overall performance of polymer electrolytes. The huge specific surface with Lewis acid sites and abundant hydroxyl groups greatly hindered the crystallization of PEO and meanwhile anchored $TFSI^-$, which contributed to great improvement in the room-temperature ionic conductivity (6.35×10^{-5} vs. 2.22×10^{-5} S cm^{-1}), Li^+ transference number (0.55 vs. 0.14), and electrochemical oxidation stability (5.0 vs. 4.2 V) of the PEO-LiTFSI electrolyte. Combined with the improvement in Young's modulus and thermostability by the zeolite nanosheet incorporation, the composite electrolyte showed higher resistance to lithium dendrite growth, increasing the cycling life of the Li||Li battery from 352 h to 2719 h. Moreover, the composite electrolyte-based LMBs demonstrated much higher capacity retention than the pristine electrolyte-based battery (93.1% vs. 37.3% after 90 cycles), indicating tremendous application potential in solid-state LMBs.

CRediT authorship contribution statement

Qian Zhao: Writing – review & editing, Writing – original draft, Visualization, Validation, Supervision, Software, Resources, Project administration, Methodology, Investigation, Funding acquisition, Formal analysis, Data curation, Conceptualization. **Jiaxin Tu:** Writing – review & editing, Writing – original draft, Visualization, Validation, Supervision, Software, Resources, Project administration, Methodology, Investigation, Funding acquisition, Formal analysis, Data curation, Conceptualization. **Rubing Xu:** Writing – review & editing, Writing – original draft, Visualization, Validation, Supervision, Software, Resources, Project administration, Methodology, Investigation, Funding acquisition, Formal analysis, Data curation, Conceptualization. **Lehao Liu:** Supervision, Project administration, Methodology, Investigation, Funding acquisition, Conceptualization. **Tianrong Yang:** Writing – original draft, Software, Formal analysis, Data curation. **Rongmin Zhou:** Writing – original draft, Software, Formal analysis, Data curation. **Dongmei Zhang:** Writing – original draft, Software, Formal analysis, Data curation. **Mengxuan Zhang:** Writing – original draft, Software, Formal analysis, Data curation. **Baoyi Wang:** Writing – original draft, Software, Formal analysis, Data curation. **Dingrong Long:** Writing – original draft, Software, Formal analysis, Data curation. **Kunda Yang:** Writing – original draft, Software, Formal analysis, Data curation. **Wei Lv:** Writing – review & editing, Visualization, Validation, Software, Methodology, Investigation, Formal analysis. **Jianan Gu:** Writing – review & editing, Visualization, Validation, Software, Methodology, Investigation, Formal analysis. **Lihua Chu:** Writing – review & editing, Visualization, Validation, Software, Methodology, Investigation, Formal analysis. **Qianxiao Fan:** Writing – review & editing, Visualization, Validation, Software, Methodology, Investigation, Formal analysis. **Ziyue Wen:** Writing – review & editing, Visualization, Validation, Software, Methodology, Investigation, Formal analysis. **Bing Jiang:** Writing – review & editing, Visualization, Validation, Software, Methodology, Investigation, Formal analysis. **Shigang Ling:** Writing – review & editing, Visualization, Validation, Software, Methodology,

Investigation, Formal analysis. **Meicheng Li:** Supervision, Project administration, Methodology, Investigation, Funding acquisition, Conceptualization.

Declaration of competing interest

The authors declare that they have no known competing financial interests or personal relationships that could have appeared to influence the work reported in this paper.

Acknowledgments

This work is supported partially by project of National Natural Science Foundation of China (52272200), Beijing Natural Science Foundation (26JL001), Hebei Natural Science Foundation (E2026502068), State Key Laboratory of Alternate Electrical Power System with Renewable Energy Sources (LAPS26007), China Three Gorges Corporation named key technologies of intelligent joint regulation and operation with grid connected friendly in power station group of wind, solar photovoltaic and energy storage (WWKY-2021-0173), Huaneng Group Headquarters Science and Technology Project (HNKJ20-H88), the Fundamental Research Funds for the Central Universities (2025MS040), and the NCEPU "Double First-Class" Program. The authors acknowledge the technology assistance of NCEPU Instrumental Analysis Center for the sample characterizations and analyses.

Appendix A. Supplementary data

Supplementary data to this article can be found online at https://doi.org/10.1016/j.est.2026.124493.

Data availability

Data will be made available on request.

References

[1] L. Liu, J. Lyu, J. Mo, H. Yan, L. Xu, P. Peng, J. Li, B. Jiang, L. Chu, M. Li, Comprehensively-upgraded polymer electrolytes by multifunctional aramid nanofibers for stable all-solid-state Li-ion batteries, Nano Energy 69 (2020) 104398, https://doi.org/10.1016/j.nanoen.2019.104398.
[2] J.B. Goodenough, Y. Kim, Challenges for rechargeable Li batteries, Chem. Mater. 22 (2010) 587–603, https://doi.org/10.1021/cm901452z.
[3] L. Han, L. Wang, Z. Chen, Y. Kan, Y. Hu, H. Zhang, X. He, Incombustible polymer electrolyte boosting safety of solid-state lithium batteries: a review, Adv. Funct. Mater. 33 (2023) 2300892, https://doi.org/10.1002/adfm.202300892.
[4] X. Meng, D. Zhang, J. Mo, L. Liu, T. Yang, Q. Fan, Q. Zhao, R. Zhou, M. Zhang, W. Hou, W. Hu, W. Zhang, Y. Jin, B. Jiang, L. Chu, M. Li, Room-temperature solid-state metallic lithium batteries based on high-content boron nitride nanosheet-modified polymer electrolytes, Appl. Surf. Sci. 648 (2024) 158962, https://doi.org/10.1016/j.apsusc.2023.158962.
[5] D. Zhang, X. Meng, W. Zhang, J. Mo, Q. Zhao, B. Wang, Q. Fan, L. Liu, T. Yang, Y. Jin, R. Zhou, M. Zhang, M. Li, A thin and ultrahigh-ionic-conductivity composite electrolyte with 3D aramid nanofiber networks toward ambient-temperature lithium metal batteries, Adv. Energy Mater. 15 (2025) 2403565, https://doi.org/10.1002/aenm.202403565.
[6] L. Liu, D. Zhang, T. Yang, W. Hu, X. Meng, J. Mo, W. Hou, Q. Fan, K. Liu, B. Jiang, L. Chu, M. Li, Flexible ion-conducting membranes with 3d continuous nanohybrid networks for high-performance solid-state metallic lithium batteries, J. Energy Chem. 75 (2022) 360–368, https://doi.org/10.1016/j.jechem.2022.08.036.
[7] L. Long, S. Wang, M. Xiao, Y. Meng, Polymer electrolytes for lithium polymer batteries, J. Mater. Chem. A 4 (2016) 10038–10069, https://doi.org/10.1039/C6TA02621D.
[8] M. Liu, D. Zhou, Y.-B. He, Y. Fu, X. Qin, C. Miao, H. Du, B. Li, Q.-H. Yang, Z. Lin, T. S. Zhao, F. Kang, Novel gel polymer electrolyte for high-performance lithium–sulfur batteries, Nano Energy 22 (2016) 278–289, https://doi.org/10.1016/j.nanoen.2016.02.008.
[9] W. Zhou, S. Wang, Y. Li, S. Xin, A. Manthiram, J.B. Goodenough, Plating a dendrite-free lithium anode with a polymer/ceramic/polymer sandwich electrolyte, J. Am. Chem. Soc. 138 (2016) 9385–9388, https://doi.org/10.1021/jacs.6b05341.
[10] J. Chai, Z. Liu, J. Ma, J. Wang, X. Liu, H. Liu, J. Zhang, G. Cui, L. Chen, In situ generation of poly (vinylene carbonate) based solid electrolyte with interfacial stability for LiCoO2 lithium batteries, Adv. Sci. 4 (2017) 1600377, https://doi.org/10.1002/advs.201600377.
[11] Q. Zhang, K. Liu, F. Ding, X. Liu, Recent advances in solid polymer electrolytes for lithium batteries, Nano Res. 10 (2017) 4139–4174, https://doi.org/10.1007/s12274-017-1763-4.
[12] J. Cheng, Y. Zhang, H. Chao, Y. Huang, H. Qin, L. Cao, X. Teng, H. Hu, M. Wu, High performance lithium-ion capacitors based on dynamic matching principle, J. Mater. Eng. 51 (2023) 29–37, https://doi.org/10.11868/j.issn.1001-4381.2021.000015.
[13] Y. He, N. Liu, P.A. Kohl, Difunctional block copolymer with ion solvating and crosslinking sites as solid polymer electrolyte for lithium batteries, J. Power Sources 481 (2021) 228832, https://doi.org/10.1016/j.jpowsour.2020.228832.
[14] X. Wang, J. Sun, C. Feng, X. Wang, M. Xu, J. Sun, N. Zhang, J. Ma, Q. Wang, C. Zong, G. Cui, Lithium bis(oxalate)borate crosslinked polymer electrolytes for high-performance lithium batteries, J. Energy Chem. 55 (2021) 228–235, https://doi.org/10.1016/j.jechem.2020.06.070.
[15] C. Liang, Z. Shi, L. Liu, J. Jin, Preparation of high performance dual network PAM/P123 gel electrolyte and application in rechargeable Zn-MnO2 batteries, J. Mater. Eng. 51 (2023) 130–139, https://doi.org/10.11868/j.issn.1001-4381.2021.000198.
[16] W. Wei, C. Liang, X. Sun, K. Wang, X. Zhang, Y. Ma, Energy storage mechanisms of metal selenides and application in lithium-ion capacitors, J. Mater. Eng. 52 (2024) 42–50, https://doi.org/10.11868/j.issn.1001-4381.2022.000922.
[17] N.T.M. Balakrishnan, A. Das, J.D. Joyner, M.J. Jabeen Fatima, L.R. Raphael, A. Pullanchiyodan, P. Raghavan, Quest for high-performance gel polymer electrolyte by enhancing the miscibility of the bi-polymer blend for lithium-ion batteries: performance evaluation in extreme temperatures, Mater. Today Chem. 29 (2023) 101407, https://doi.org/10.1016/j.mtchem.2023.101407.
[18] D. Devaux, D. Glé, T. Phan, D. Gigmes, E. Giroud, M. Deschamps, R. Denoyel, R. Bouchet, Optimization of block copolymer electrolytes for lithium metal batteries, Chem. Mater. 27 (2015) 4682–4692, https://doi.org/10.1021/acs.chemmater.5b01273.
[19] P. Pradeepa, S. Edwin raj, G. Sowmya, J. Kalaiselvimary, M. Ramesh Prabhu, Optimization of hybrid polymer electrolytes with the effect of lithium salt concentration in PEO/PVDF-HFP blends, Mater. Sci. Eng. B 205 (2016) 6–17, https://doi.org/10.1016/j.mseb.2015.11.009.
[20] M.S. Grewal, M. Tanaka, H. Kawakami, Bifunctional poly(ethylene glycol) based crosslinked network polymers as electrolytes for all-solid-state lithium ion batteries, Polym. Int. 68 (2019) 684–693, https://doi.org/10.1002/pi.5750.
[21] Z. Li, Y. You, X. Liang, P. Wang, Z. Zhang, X. Du, B. Liu, Z. Sun, W. Hu, A single ion polymer electrolyte via copolymerization of lithium (4-styrenesulfonyl)(trifluoromethanesulfonyl)imide and allyl poly(aryl ether ketone) enables safe lithium ion Batteries, Appl. Surf. Sci. 611 (2023) 155363, https://doi.org/10.1016/j.apsusc.2022.155363.
[22] M. Watanabe, T. Hirakimoto, S. Mutoh, A. Nishimoto, Polymer electrolytes derived from dendritic polyether macromonomers, Solid State Ion. 148 (2002) 399–404, https://doi.org/10.1016/S0167-2738(02)00079-6.
[23] J. Li, G. Chang, L. Xu, T. Gao, J. Ma, D. Zhan, X. Lu, EC modified PEO/PVDF-LLZO composite electrolytes for solid state lithium metal batteries, J. Indian Chem. Soc. 100 (2023) 100959, https://doi.org/10.1016/j.jics.2023.100959.
[24] K. Xie, L. Shi, Ultrathin PEO based electrolyte for high voltage lithium metal batteries enabled by polymer host-plasticizer interactions, J. Energy Storage 68 (2023) 107640, https://doi.org/10.1016/j.est.2023.107640.
[25] Y. Guo, E. Zhao, X. Zhao, S. Liu, One dimensional CeO_2 nanorods/poly(ethylene oxide) solid composite electrolyte for all-solid-state lithium-ion batteries, J. Rare Earths 42 (2024) 570–577, https://doi.org/10.1016/j.jre.2023.06.006.
[26] H. Hou, B. Huang, X. Yu, J. Lan, S. Ming, J. Rong, X. Liu, F. Chen, Compatible composite electrolyte membrane $Li_7La_3Zr_2O_{12}$/SB-PVDF for solid-state lithium ion battery, J. Energy Storage 68 (2023) 107680, https://doi.org/10.1016/j.est.2023.107680.
[27] F. Li, B. Su, L. Shi, J. Mu, F. Xu, J. Wang, H. Yang, Z. Guo, Hybrid poly(ethylene oxide)-based composite polymer electrolyte for high-performance all-solid-state lithium batteries, Ceram. Int. 49 (2023) 26604–26615, https://doi.org/10.1016/j.ceramint.2023.05.195.
[28] Z. Ding, Q. Tang, Q. Zhang, P. Yao, X. Liu, J. Wu, A flexible solid polymer electrolyte enabled with lithiated zeolite for high performance lithium battery, Nano Res. 16 (2023) 9443–9452, https://doi.org/10.1007/s12274-023-5658-2.
[29] Y. Wang, L. Wu, Z. Lin, M. Tang, P. Ding, X. Guo, Z. Zhang, S. Liu, B. Wang, X. Yin, Z. Chen, K. Amine, H. Yu, Hydrogen bonds enhanced composite polymer electrolyte for high-voltage cathode of solid-state lithium battery, Nano Energy 96 (2022) 107105, https://doi.org/10.1016/j.nanoen.2022.107105.
[30] H. Jiang, Y. Du, L. Zhao, X. Liu, J. Kong, P. Liu, T. Zhou, Mof-derived ionic conductor enhancing the performance of polymer electrolyte for solid-state lithium batteries, Chem. Eng. J. 487 (2024) 150455, https://doi.org/10.1016/j.cej.2024.150455.
[31] L. Wang, Y. Zhong, Z. Wen, C. Li, J. Zhao, M. Ge, P. Zhou, Y. Zhang, Y. Tang, G. Hong, A strong Lewis acid imparts high ionic conductivity and interfacial stability to polymer composite electrolytes towards all-solid-state li-metal batteries, Sci. China-Mater. 65 (2022) 2179–2188, https://doi.org/10.1007/s40843-021-1908-x.
[32] X. Ji, Y. Zhang, M. Cao, Q. Gu, H. Wang, J. Yu, Z.-H. Guo, X. Zhou, Advanced Inorganic/polymer Hybrid Electrolytes for All-solid-state Lithium Batteries, J. Adv. Ceram. 11 (2022) 835–861, https://doi.org/10.1007/s40145-022-0580-8.
[33] S. Liu, W. Liu, D. Ba, Y. Zhao, Y. Ye, Y. Li, J. Liu, Filler-integrated composite polymer electrolyte for solid-state lithium batteries, Adv. Mater. 35 (2023) 2110423, https://doi.org/10.1002/adma.202110423.

[34] K. Na, W. Park, Y. Seo, R.J.C.o.M. Ryoo, Disordered assembly of MFI zeolite nanosheets with a large volume of intersheet mesopores, Chem. Mater. 23 (2011) 1273–1279, https://doi.org/10.1021/cm103245m.
[35] E. Verheyen, C. Jo, M. Kurttepeli, G. Vanbutsele, E.R. Gobechiya, T.I. Korányi, S. Bals, G.v. Tendeloo, R. Ryoo, C.E.A. Kirschhock, J.A. Martens, Molecular shape-selectivity of MFI zeolite nanosheets in N-decane isomerization and hydrocracking, J. Catal. 300 (2013) 70–80, https://doi.org/10.1016/j.jcat.2012.12.017.
[36] L. Emdadi, Y. Wu, G. Zhu, C.-C. Chang, W. Fan, T. Pham, R.F. Lobo, D. Liu, Dual template synthesis of meso- and microporous MFI zeolite nanosheet assemblies with tailored activity in catalytic reactions, Chem. Mater. 26 (2014) 1345–1355, https://doi.org/10.1021/cm401119d.
[37] M. Choi, K. Na, J. Kim, Y. Sakamoto, O. Terasaki, R. Ryoo, Stable single-unit-cell nanosheets of zeolite MFI as active and long-lived catalysts, Nature 461 (2009) 246–249, https://doi.org/10.1038/nature08288.
[38] B. Bensafi, N. Chouat, F. Djafri, The universal zeolite ZSM-5: structure and synthesis strategies. A review, Coord. Chem. Rev. 496 (2023) 215397, https://doi.org/10.1016/j.ccr.2023.215397.
[39] J. Li, S. Bi, T. Duan, Y. Liu, Q. Sun, T. Hu, X. Lu, H. Cheng, Boosting Li^+ transport in ultra-stable all-solid-state lithium metal batteries via bimetal oxide enhanced $PrBaCoFeO_{5+\delta}$ perovskite nanofillers, Nano Res. 19 (2026) 94908178, https://doi.org/10.26599/nr.2025.94908178.
[40] J. Li, L. Chang, J. Liu, Q. Sun, X. Lu, H. Cheng, Decoupling and reconstructing multiscale ion transport in PEO-based composite electrolytes via thermodynamics, kinetics, and rational design, Energy Storage Mater. 84 (2026) 104887, https://doi.org/10.1016/j.ensm.2026.104887.
[41] Z. Lei, J. Shen, W. Zhang, Q. Wang, J. Wang, Y. Deng, C. Wang, Exploring porous Zeolitic Imidazolate Frame Work-8 (ZIF-8) as an efficient filler for high-performance poly(ethyleneoxide)-based solid polymer electrolytes, Nano Res. 13 (2020) 2259–2267, https://doi.org/10.1007/s12274-020-2845-2.
[42] A.S. Al-Dughaither, H. de Lasa, HZSM-5 zeolites with different SiO_2/Al_2O_3 ratios. Characterization and NH_3 desorption kinetics, Ind. Eng. Chem. Res. 53 (2014) 15303–15316, https://doi.org/10.1021/ie4039532.
[43] Y. Tao, W. Wei, Q. Gu, X. Jiang, D.J.M.L. Li, Desilicated zeolite ZSM-5 based composite polymer electrolytes for solid-state lithium metal batteries, Mater. Lett. 351 (2023) 134934, https://doi.org/10.1016/j.matlet.2023.134934.
[44] M. Yang, J. Zhang, Z. Ren, B. Wang, H. Li, J. Cheng, Li_2CO_3/LiF-rich solid electrolyte interface stabilized lithium metal anodes for durable Li-CO_2 batteries, Energy Storage Mater. 73 (2024) 103843, https://doi.org/10.1016/j.ensm.2024.103843.
[45] C. Han, H. Shen, M. Li, Y. Tian, Y. Chen, X. Wu, J. Sun, L. Liu, X. Zhang, J. Tang, Y. He, Y. Li, M. Xie, Z. Li, Nano-confined synergistic conduction enables electrolytes for all-solid-state lithium metal batteries, Adv. Funct. Mater. 36 (2025) e23139, https://doi.org/10.1002/adfm.202523139.
[46] L. Yang, H. Zhang, E. Xia, Y. Wu, Z. Li, PEO/Li_2ZrO_3 composite electrolyte for solid-state rechargeable lithium battery, J. Energy Storage 65 (2023) 107283, https://doi.org/10.1016/j.est.2023.107283.
[47] J. Cheng, G. Hou, Q. Chen, D. Li, K. Li, Q. Yuan, J. Wang, L. Ci, Sheet-like garnet structure design for upgrading PEO-based electrolyte, Chem. Eng. J. 429 (2022) 132343, https://doi.org/10.1016/j.cej.2021.132343.
[48] E. Zhao, Y. Guo, Y. Liu, S. Liu, G. Xu, Nanostructured Zeolitic Imidazolate Framework-67 reinforced poly(ethylene oxide) composite electrolytes for all solid state lithium ion batteries, Appl. Surf. Sci. 573 (2022) 151489, https://doi.org/10.1016/j.apsusc.2021.151489.
[49] L. Chen, X. Qiu, Z. Bai, L.-Z. Fan, Enhancing interfacial stability in solid-state lithium batteries with polymer/garnet solid electrolyte and composite cathode framework, J. Energy Chem. 52 (2021) 210–217, https://doi.org/10.1016/j.jechem.2020.03.052.
[50] L. Tian, Y. Liu, Z. Su, Y. Cao, W. Zhang, S. Yi, Y. Zhang, B. Niu, P. Dong, D. Long, A lithiated organic nanofiber-reinforced composite polymer electrolyte enabling Li-ion conduction highways for solid-state lithium metal batteries, J. Mater. Chem. A 9 (2021) 23882–23890, https://doi.org/10.1039/d1ta06269g.
[51] C. Li, Y. Huang, X. Feng, Z. Zhang, H. Gao, J. Huang, Silica-assisted cross-linked polymer electrolyte membrane with high electrochemical stability for lithium-ion batteries, J. Colloid Interface Sci. 594 (2021) 1–8, https://doi.org/10.1016/j.jcis.2021.02.128.
[52] X. Yin, L. Wang, Y. Kim, N. Ding, J. Kong, D. Safanama, Y. Zheng, J. Xu, D.V. M. Repaka, K. Hippalgaonkar, S.W. Lee, S. Adams, G.W. Zheng, Thermal conductive 2D boron nitride for high-performance all-solid-state lithium–sulfur batteries, Adv. Sci. 7 (2020) 2001303, https://doi.org/10.1002/advs.202001303.
[53] T.-Q. Yang, C. Wang, W.-K. Zhang, Y. Xia, Y.-P. Gan, H. Huang, X.-P. He, J. Zhang, Composite polymer electrolytes reinforced by a three-dimensional polyacrylonitrile/$Li_{0.33}La_{0.557}TiO_3$ nanofiber framework for room-temperature dendrite-free all-solid-state lithium metal battery, Rare Metals 41 (2022) 1870–1879, https://doi.org/10.1007/s12598-021-01891-1.
[54] A. Chen, Q. Zeng, W. Wen, X. Wen, Z. Li, Y. Liu, J. Guan, H. Wang, W. Liu, P. Chen, L. Zhang, A highly salt-soluble ketone-based all-solid-state polymer electrolyte with superior performances for lithium-ion batteries, ACS Appl. Mater. Interfaces 15 (2023) 17791–17800, https://doi.org/10.1021/acsami.2c22228.
[55] E. Zhao, Y. Guo, A. Zhang, H. Wang, G. Xu, Polydopamine coated TiO_2 nanofiber fillers for polyethylene oxide hybrid electrolytes for efficient and durable all solid state lithium ion batteries, Nanoscale 14 (2022) 890–897, https://doi.org/10.1039/d1nr06636f.
[56] Y. Li, Y. Qin, J. Zhao, M. Ma, M. Zhang, P. Li, S. Lu, H. Bu, K. Xi, Y. Su, S. Ding, Boosting the ion mobility in solid polymer electrolytes using hollow polymer nanospheres as an additive, ACS Appl. Mater. Interfaces 14 (2022) 18360–18372, https://doi.org/10.1021/acsami.2c00244.
[57] T.I. Kolesnikov, D. Voll, F. Jeschull, P. Theato, Synthesis of polyimide-PEO copolymers: toward thermally stable solid polymer electrolytes for lithium-metal batteries, Eur. Polym. J. 217 (2024) 113315, https://doi.org/10.1016/j.eurpolymj.2024.113315.
[58] L. Bertoli, G. Gabriele, E. Gibertini, L. Magagnin, Unconventional PEO-PPC quasi-solid state blend polymer electrolyte for high efficiency solid-state Li-metal batteries, J. Energy Storage 81 (2024) 110456, https://doi.org/10.1016/j.est.2024.110456.
[59] Z. Hu, X. Jing, M. Chen, H. Xu, Y. Zhang, H. Cheng, Multifunctional single-ion conductor-integrated PEO-based solid polymer electrolytes endow highly stable and dendrite-free lithium metal batteries, Next Mater. 2 (2024) 100090, https://doi.org/10.1016/j.nxmate.2023.100090.
[60] L. Chen, X. Liu, G. Zang, J. Xie, B. Wu, C. Zhang, Y. Xu, Y. Luo, D. Yu, Z. Zhang, A new strategy through polymer in situ ionization to construct high-performance electrolyte for solid-state batteries, J. Energy Chem. 105 (2025) 814–822, https://doi.org/10.1016/j.jechem.2025.01.025.
[61] H. Hu, J. Li, Y. Wu, W. Fang, H. Zhang, X. Ji, Revealing the role and working mechanism of confined ionic liquids in solid polymer composite electrolytes, J. Energy Chem. 99 (2024) 110–119, https://doi.org/10.1016/j.jechem.2024.07.027.
[62] L. Liu, J. Mo, R. Zhou, T. Yang, R. Xu, J. Tu, Q. Zhao, M. Zhang, D. Zhang, B. Wang, D. Long, K. Yang, J. Zhang, M. Li, Ultrathin solid composite electrolytes for long-life lithium metal batteries, J. Energy Storage 114 (2025) 115777, https://doi.org/10.1016/j.est.2025.115777.